



## Supporting Information

for *Small*, DOI: 10.1002/smll.201604179

Aligned Growth of Millimeter-Size Hexagonal Boron Nitride  
Single-Crystal Domains on Epitaxial Nickel Thin Film

*Junhua Meng, Xingwang Zhang,\* Ye Wang, Zhigang Yin,  
Heng Liu, Jing Xia, Haolin Wang, Jingbi You, Peng Jin,  
Denggui Wang, and Xiang-Min Meng*

## Supporting Information

**Aligned Growth of Millimeter-Size Hexagonal Boron Nitride Single-Crystal Domains on Epitaxial Nickel Thin Film**

*Junhua Meng, Xingwang Zhang,\* Ye Wang, Zhigang Yin, Heng Liu, Jing Xia, Haolin Wang, Jingbi You, Peng Jin, Denggui Wang, and Xiang-Min Meng*

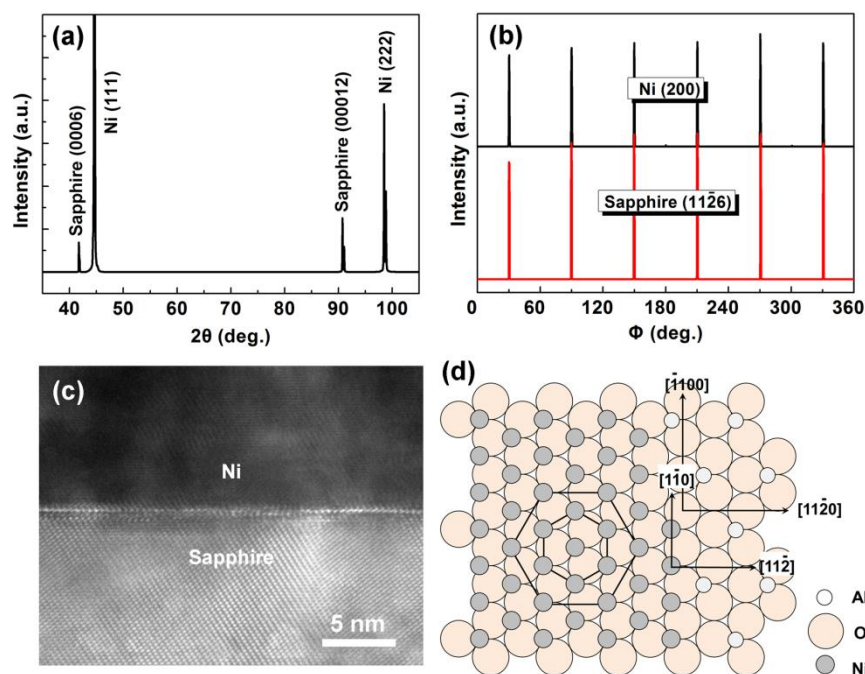


**Figure S1.** Characterization of the epitaxial Ni films on sapphire (0001) substrates. (a) XRD pattern of the Ni film on sapphire (0001). (b)  $\Phi$  scans of the Ni (200) reflections and the sapphire (112̄6) reflections of the Ni film on sapphire. (c) Cross-sectional TEM of the epitaxial Ni film on sapphire. (d) Schematic of the atom positions and epitaxial relationship between Ni film and sapphire (0001): Ni (111)[112̄]//sapphire (0001)[1120].

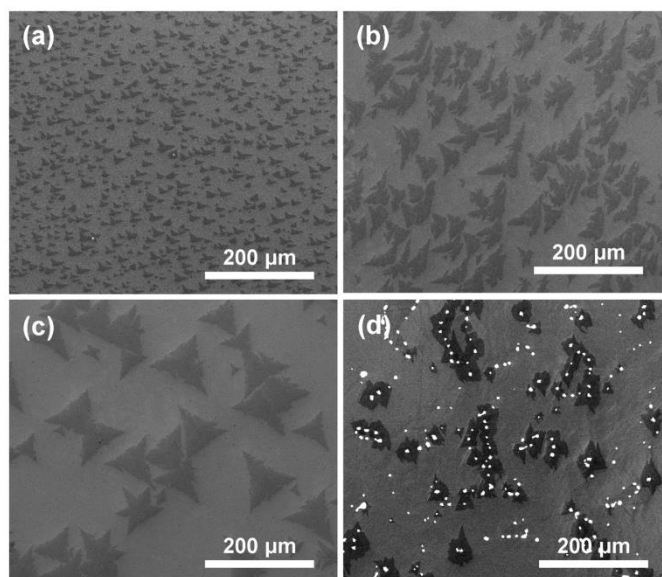


**Figure S2.** SEM images of the h-BN domains prepared at different temperatures. The h-BN domains were prepared on a 0.5  $\mu\text{m}$  thick Ni film with an ion beam density of 0.1  $\text{mA cm}^{-2}$  at (a) 850, (b) 950, (c) 1050, and (d) 1150  $^{\circ}\text{C}$ , respectively. The largest size of h-BN domains was obtained at 1050  $^{\circ}\text{C}$ , while a large amount of defects appears on the Ni surface with further increasing growth temperature to 1150  $^{\circ}\text{C}$ .

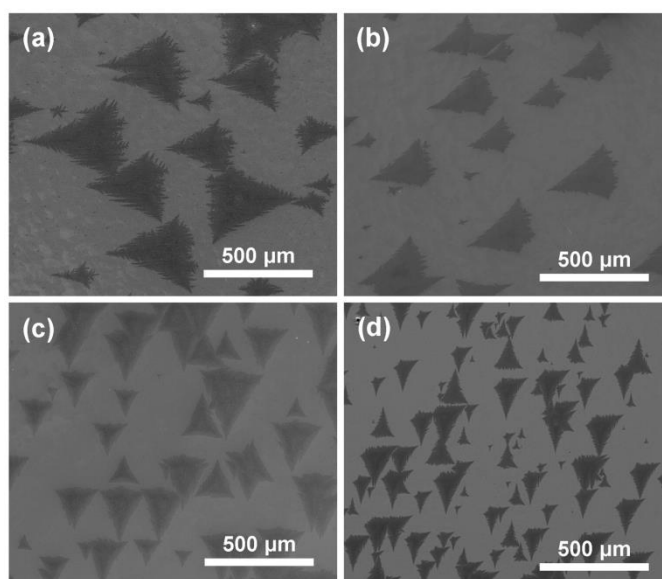


**Figure S3.** SEM images of the h-BN domains prepared with different ion beam densities. The h-BN domains were prepared on a 1.2  $\mu\text{m}$  thick Ni film at 1050  $^{\circ}\text{C}$  with ion beam densities of (a) 0.1, (b) 0.2, (c) 0.3, and (d) 0.4  $\text{mA cm}^{-2}$ , respectively. The flux of BN species, which is monitored by a quartz crystal oscillator at room temperature, is corresponded to 0.08, 0.16, 0.23, 0.30  $\text{nm/min}$ , respectively. The largest size of h-BN domains was obtained with an ion beam density of 0.1  $\text{mA cm}^{-2}$ . The growth mode of h-BN domains on the catalyst surface by the diffusion of the constituent species or by the incorporation kinetics of the constituent species. The diffusion instabilities with the lower ion beam density lead to more dendritic domain growth, as shown in Figure S3a.

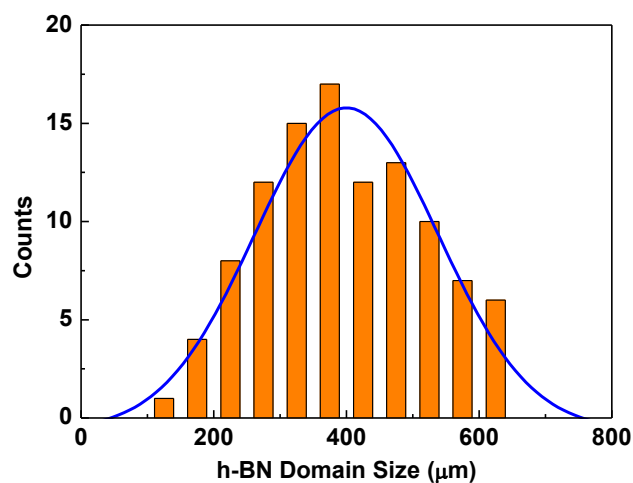


**Figure S4.** The statistic plot of the size distribution of h-BN domains under the optimized condition.

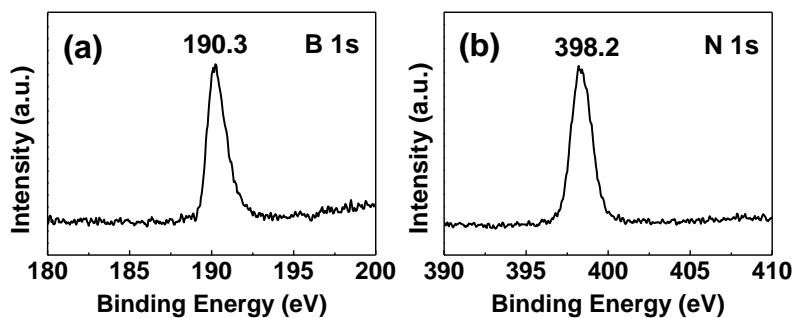


**Figure S5.** XPS spectra of h-BN. (a) B 1s and (b) N 1s core-level XPS spectra with binding energies peaks at 190.3 and 398.2 eV. The B:N elemental stoichiometry extracted from the integral intensities of the characteristic peaks is 1:1.03.

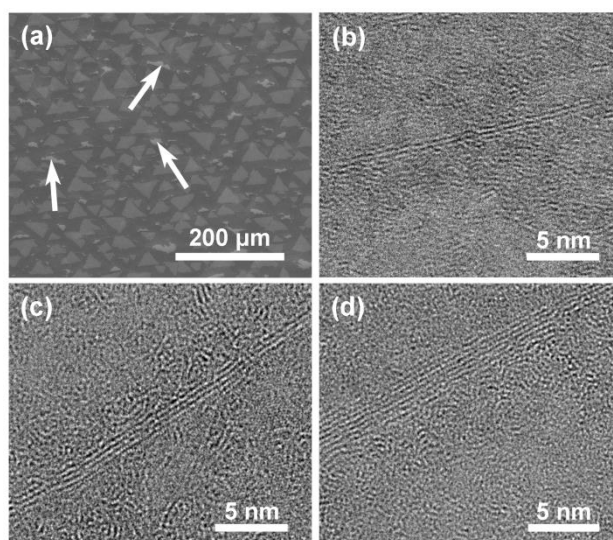


**Figure S6.** SEM and Cross-sectional view HRTEM images of bilayer and few-layer h-BN domains. For the samples synthesized with the ion beam density of  $0.7 \text{ mA cm}^{-2}$ , bi-layer h-BN sheets were typically observed from (a) SEM and (b) TEM images, (c,d) few-layer h-BN sheets were also occasionally observed. The triangular h-BN domains (the second layer) with the lighter colour was grown on the first h-BN layer (darker colour), while the white arrows indicate the occasionally observed bare Ni substrate.

**Effect of Ni thickness on h-BN growth:** The segregation and precipitation of C atoms on Ni is a widely proposed mechanism for the formation of graphene using CVD, and thus, the thickness of Ni film plays an important role for the growth of graphene on Ni. Unlike graphene, the growth mechanism of h-BN on Ni is dominated by surface-mediated reaction in the case of IBSD, and the direct influence of the Ni thickness on h-BN growth is negligible. However, with the increase of Ni thickness, the density of grain boundaries significantly decreases, leading to a reduced roughness of Ni surface. Consequently, the nucleation density of h-BN decreases and their sizes increase with the Ni thickness.

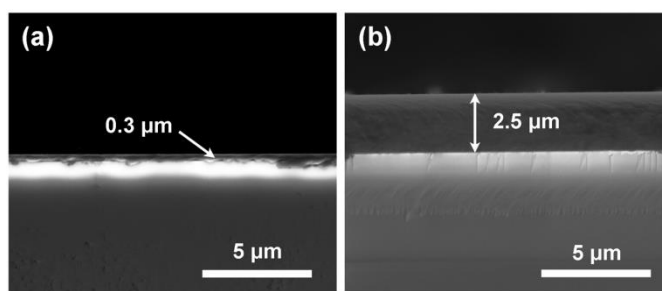


**Figure S7.** Cross-sectional SEM images of two epitaxial Ni films with different thicknesses. The thicknesses of Ni films are determined to be (a) 0.3 and (b) 2.5  $\mu\text{m}$  from the SEM images, respectively.

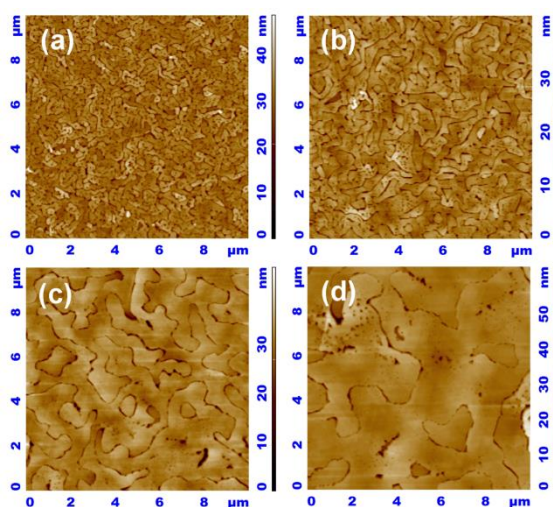


**Figure S8.** AFM images of the as-grown Ni films with different thicknesses on sapphire (0001). The thickness of Ni films are (a) 0.3, (b) 0.7, (c) 1.2 and (d) 2.0  $\mu\text{m}$ , respectively.

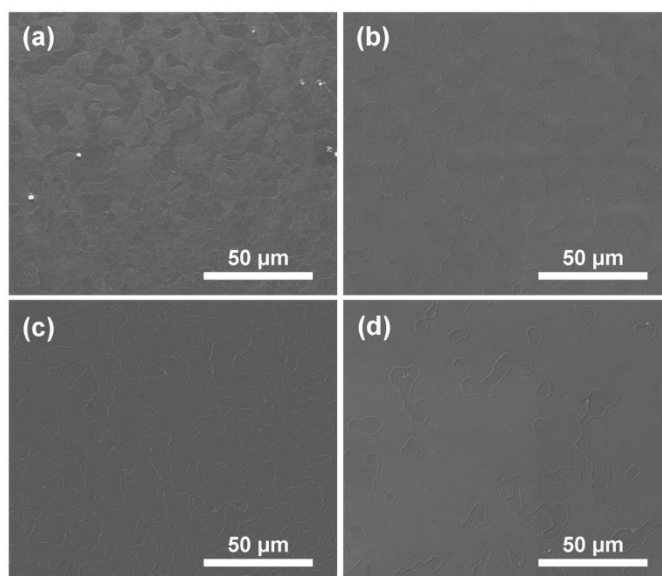


**Figure S9.** SEM images of the annealed Ni films with different thicknesses. The thickness of Ni films are (a) 0.3, (b) 0.7, (c) 1.2 and (d) 2.0  $\mu\text{m}$ , respectively.



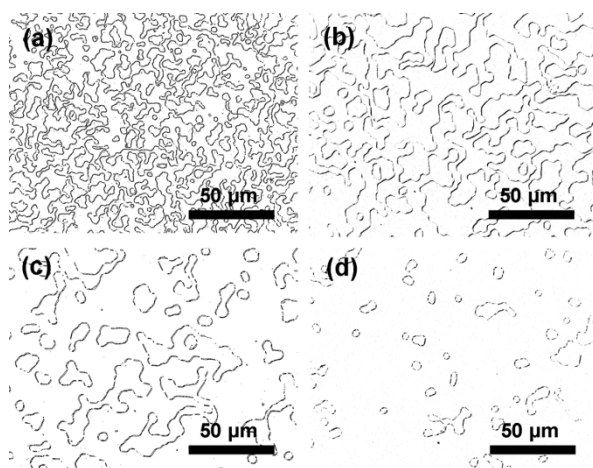


**Figure S10.** Black-white images converted from the optical microscopy images in Figure 4a-d by applying an appropriated grey level threshold with ImageJ software. The process of extracting the length of Ni-grain boundaries from the optical microscopy images of the Ni films by ImageJ software is described as follows. First, the optical microscopy images in Figure 4a-d were converted into black-white images by applying an appropriated grey level threshold with ImageJ software, as shown in Figure S10. The Ni-grain boundaries are shown as black contour lines on a white background. Then the lengths of Ni-grain boundaries were determined by summing the black pixels in Figure S10.

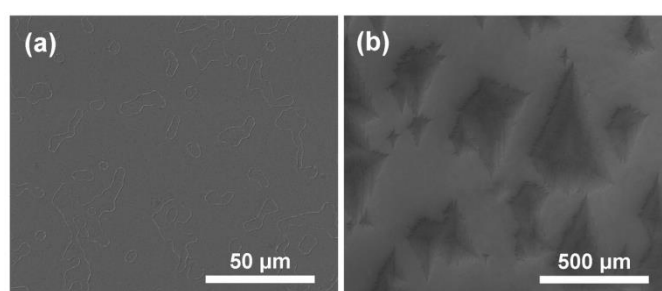


**Figure S11.** The h-BN domains grown on a 2.5  $\mu\text{m}$  thick Ni film. (a) SEM image of the annealed 2.5  $\mu\text{m}$  thick Ni films before the growth of h-BN. (b) SEM image of the h-BN domains synthesized on a 2.5  $\mu\text{m}$  thick Ni film at 1050  $^{\circ}\text{C}$  with an ion beam density of 0.1  $\text{mA cm}^{-2}$ .